Materials Advances

ROYAL SOCIETY OF CHEMISTRY

COMMUNICATION

View Article Online
View Journal | View Issue

Cite this: *Mater. Adv.*, 2024, 5, 123

Received 29th April 2023,
Accepted 31st August 2023

DOI: 10.1039/d3ma00202k

rsc.li/materials-advances

Three-dimensional lead iodide perovskites based on complex ions†

Hebin Wang,‡[a] Yinye Yu,‡[bcd] Haolin Lu,[a] Teng Wang,[a] Yuki Haruta,[e] Xingzhan Wei,[c] Guichuan Xing,[f] Makhsud I. Saidaminov,[g] Yecheng Zhou *[b] and Guankui Long *[a]

Lead-halide perovskites have demonstrated outstanding optical, electrical, and spintronic properties and have made significant breakthroughs in many fields, especially in solar cells. Although substantial efforts have been devoted to developing novel 3D perovskites with a lower band gap towards the application in perovskite solar cells, none of them succeeded. Here we propose three novel 3D lead iodide perovskites with complex ions, $Cu(NH_3)_2PbI_3$, $Ag(NH_3)_2PbI_3$ and $Au(NH_3)_2PbI_3$. Based on the optimized structures, formation and dissociation energies, phonon spectra, and *ab initio* molecular dynamics simulations, it is found that $Ag(NH_3)_2PbI_3$ and $Au(NH_3)_2PbI_3$ are kinetically and thermodynamically stable. Furthermore, $Ag(NH_3)_2PbI_3$ and $Au(NH_3)_2PbI_3$ exhibit large absorption coefficients, suitable optical band gaps and small electron effective masses, which are very promising towards application in perovskite solar cells.

Introduction

The lead-halide perovskites with ABX_3 structures have attracted attention owing to their unique optical, electrical, and spintronic properties towards applications in solar cells,[1–11] light-emitting diodes,[9,12–14] photodetectors,[15–18] field-effect transistors,[19] lasers,[20,21] *etc.* The power conversion efficiency (PCE) of lead-halide perovskite solar cells has exceeded 25%,[2] which is comparable to that of the commercialized silicon-based solar cells. Taking the crystal structure into account, perovskites can be categorized by the arrangement of metal halide octahedra into different dimensionalities such as three-dimensional (3D),[22–25] two-dimensional (2D),[4,26–28] one-dimensional (1D),[29,30] and zero-dimensional (0D).[31–34] The dimensionality can be tuned by the size of the A-site cations. The cations can also influence the electronic properties of perovskite through distortions and symmetry breaking.[35–42] To understand the unique optical and charge transport properties of 3D perovskites, not only structural but also electronic dimensionality – the connectivity of the conduction band (CB) and valence band (VB),[43] is important. Structural 3D does not always lead to electronic 3D (such as $Cs_2AgBiBr_6$[43]), while electronic 3D can only be achieved in 3D perovskites. The electronic dimensionality is determined by complex factors, such as the structural dimensionality, structural distortion, and the contribution of the A-site cations and inorganic framework to the VBM and CBM.[43] The 3D electronic structure could ensure the isotropic charge transport in the crystal lattice. For 3D perovskites with 3D electronic connectivity, the charges can freely move along three dimensions since both the VB and CB are dispersive along all directions rather than restricted to one or two directions in electronically low-dimensional perovskites. Considering the randomly oriented grains in the perovskite thin film and the need for effective hole and electron transport between electrodes, the excellent isotropic transport of electronic 3D perovskites could ensure effective charge transport and hence high power conversion efficiency.

For solar cell applications, there are three types of widely investigated 3D lead iodide perovskites: $CH_3NH_3PbI_3$ ($MAPbI_3$), $NH_2CHNH_2PbI_3$ ($FAPbI_3$) and $CsPbI_3$, with band gaps of 1.57 eV, 1.48 eV and 1.73 eV, respectively.[44] But according to the Shockley–Queisser limit, a 1.34 eV band gap leads to the

[a] *School of Materials Science and Engineering, National Institute for Advanced Materials, Renewable Energy Conversion and Storage Center (RECAST), Nankai University, 300350, Tianjin, China. E-mail: longgk09@nankai.edu.cn*
[b] *School of Materials Science and Engineering, Sun Yat-sen University, Guangzhou 510006, China. E-mail: zhouych29@mail.sysu.edu.cn*
[c] *Micro-nano Manufacturing and System Integration Center, Chongqing Institute of Green and Intelligent Technology, Chinese Academy of Sciences, Chongqing 400714, China*
[d] *University of Chinese Academy of Sciences, No. 19A Yuquan Road, Shijingshan District, Beijing 100049, China*
[e] *Department of Chemistry, University of Victoria, Victoria, British Columbia V8P 5C2, Canada*
[f] *Institute of Applied Physics and Materials Engineering, University of Macau, Avenida da Universidade, Taipa, Macau, 999078, China*
[g] *Department of Chemistry, Department of Electrical & Computer Engineering, and Centre for Advanced Materials and Related Technologies (CAMTEC), University of Victoria, Victoria, British Columbia V8P 5C2, Canada*

† Electronic supplementary information (ESI) available. See DOI: https://doi.org/10.1039/d3ma00202k

‡ These authors contributed equally to this work.

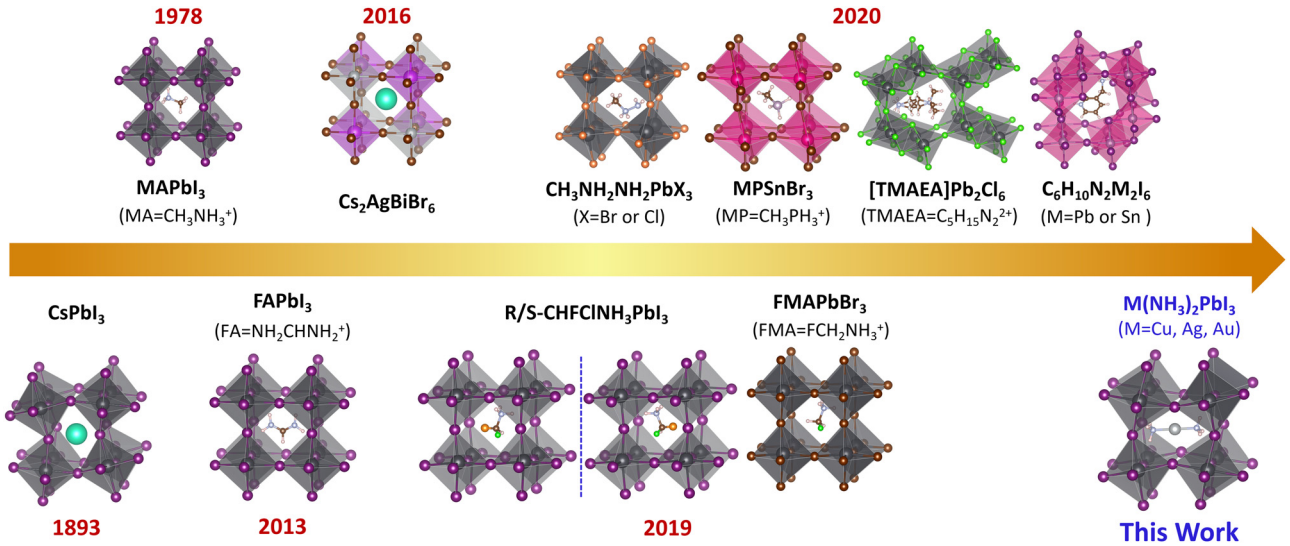

Fig. 1 Summary of the important milestones of 3D hybrid halide perovskites.

best performing solar cells;[45] therefore, it is highly needed to develop novel 3D perovskites with a lower band gap. However, such an ideal 3D lead iodide perovskite has not been developed although various novel 3D perovskites have been proposed, as shown in Fig. 1. For example, double perovskites like $Cs_2AgBiBr_6$[46–48] and $(CH_3NH_3)_2BiKCl_6$[49] were reported, but they have indirect band gaps (2.19 eV and 3.04 eV) and 0D electronic structure,[43] and the highest power conversion efficiency is only 2.5% for these double perovskite-based solar cells.[50] Later, Xiong *et al.* synthesized methylphosphonium ($CH_3PH_3^+$, MP^+)-based hybrid organic–inorganic perovskites ($MPSnBr_3$, with a large band gap of 2.62 eV), which were proven to be structural 3D based on single crystal X-ray diffraction.[51] Mączka *et al.* reported novel 3D lead chloride and bromide perovskites with large band gaps of 3.40 eV and 2.58 eV based on 2-methylhydrazin-1-ium ($CH_3NHNH_3^+$).[52] Long *et al.* proposed the 3D chiral lead iodide perovskite ($CHFClNH_3PbI_3$), which was proven to be both kinetically and thermodynamically stable based on theoretical calculations.[24] Zhong *et al.* experimentally reported the first halogenated-methylammonium-based 3D lead halide perovskite ($FMAPbBr_3$) with a band gap of 2.03 eV.[53] Recently, a series of unique 3D lead halide perovskites based on diammonium and edge-shared $(Pb_2X_{10})^{6-}$ octahedra dimers were also reported.[54–59] For example, Xiong *et al.* developed a 3D ferroelectric lead-based perovskite ($[TMAEA]Pb_2Cl_6$, TMAEA = 2-trimethylammonioethylammonium), which exhibits a large band gap of 3.43 eV and spontaneous polarization of 1 μC cm^{-2}.[54] Kanatzidis *et al.* reported 3D lead-based perovskites ($(x$AMPY$)Pb_2I_6$, x = 3 or 4, AMPY = aminomethylpyridinium) with indirect band gaps of 2.05 eV (x = 3) and 2.12 eV (x = 4).[55] However, all these experimentally reported novel 3D lead halide perovskites exhibit large band gaps (>2.0 eV), which could not harvest enough photons towards high-performance perovskite solar cells.

In this work, we introduce three complex ions, $[Cu(NH_3)_2]^+$, $[Ag(NH_3)_2]^+$ and $[Au(NH_3)_2]^+$, to construct novel 3D lead-based perovskites. Based on the optimized structures, formation and dissociation energies, phonon spectra, and *ab initio* molecular dynamics simulations (AIMD), it is found that $Ag(NH_3)_2PbI_3$ and $Au(NH_3)_2PbI_3$ are both kinetically and thermodynamically stable. Most importantly, these two perovskites are not only structural 3D but also electronic 3D. With high absorption coefficients, low band gaps, and small hole and electron effective masses, $Ag(NH_3)_2PbI_3$ and $Au(NH_3)_2PbI_3$ are very promising towards potential applications in perovskite solar cells.

Results and discussion

The geometric structures of the proposed lead-based perovskites with complex ions, $[Cu(NH_3)_2]^+$, $[Ag(NH_3)_2]^+$ and $[Au(NH_3)_2]^+$, are optimized and shown in Fig. 2. The 3D structures are not destroyed after the introduction of complex ions, indicating that $[Cu(NH_3)_2]^+$, $[Ag(NH_3)_2]^+$ and $[Au(NH_3)_2]^+$ are successfully embedded into the perovskite lattice framework without destroying the 3D structure. In order to further confirm this, the new tolerance factors (τ_{au}) proposed by Bartel *et al.* were calculated.[60,61] As shown in Table S1 (ESI†), the calculated τ_{au} is 3.57, 3.58 and 3.57 for $Cu(NH_3)_2PbI_3$, $Ag(NH_3)_2PbI_3$ and $Au(NH_3)_2PbI_3$, respectively, which is almost the same as that of $FAPbI_3$ (3.64), further confirming that the proposed lead iodide perovskites could maintain their 3D structures. The average Pb–I bond lengths of $Cu(NH_3)_2PbI_3$, $Ag(NH_3)_2PbI_3$ and $Au(NH_3)_2PbI_3$ are 3.28, 3.24 and 3.26 Å, respectively, which is comparable with that of 3.22 Å in γ-$MAPbI_3$.[24] To further estimate the distortion of the three perovskites with complex ions, the bond length distortion index (D), the bond angle variance (σ^2) and the angle of the Pb–I–Pb bond (in-plane of (010)) were calculated. D and σ^2 estimate the distortion degree of the $[PbI_6]^{4-}$ octahedra, and the Pb–I–Pb bond angle (in-plane of (010)) estimates the degree of octahedral tilting in the perovskites. As shown in Table S4 and Fig. S1 (ESI†), the D values of

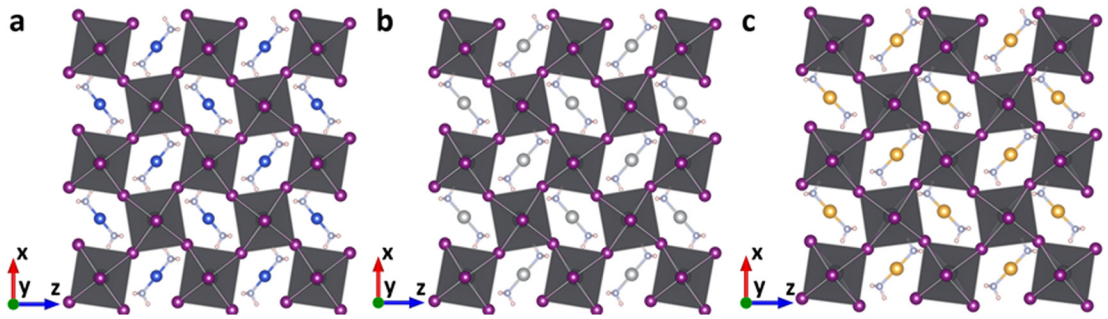

Fig. 2 The optimized geometric structures of $Cu(NH_3)_2PbI_3$ (a), $Ag(NH_3)_2PbI_3$ (b) and $Au(NH_3)_2PbI_3$ (c).

$Cu(NH_3)_2PbI_3$, $Ag(NH_3)_2PbI_3$ and $Au(NH_3)_2PbI_3$ are much larger than that of γ-$MAPbI_3$, while σ^2 is in the order of $Cu(NH_3)_2PbI_3$ < $Ag(NH_3)_2PbI_3$ < γ-$MAPbI_3$ < $Au(NH_3)_2PbI_3$. The tilting distortions of $Cu(NH_3)_2PbI_3$, $Ag(NH_3)_2PbI_3$ and $Au(NH_3)_2PbI_3$ are much smaller than that of γ-$MAPbI_3$. The stability of these proposed 3D perovskites with complex ions is further investigated by the phonon spectra, formation and dissociation energies, and *ab initio* molecular dynamics simulations, as shown below.

As shown in Fig. 3a–c, all these perovskites exhibit a similar phonon spectrum, and only very small imaginary frequencies (<2 THz) are found. These small imaginary modes are a very common feature for lead-based perovskites[62] and have been confirmed by the soft mode in experiments (*e.g.*, $MAPbBr_3$)[63] and theoretical calculations (*e.g.*, α-$MAPbI_3$).[64–69] The origin of the imaginary frequencies is potentially due to the anharmonicity,[64,65] which is caused by the rotations and tilting of the octahedra,[62,66] or dynamic stabilization.[67–72] The vibration modes that arise from the imaginary phonon frequencies were also analyzed. As shown in Fig. S2 (ESI†), the I(5) atom of $Cu(NH_3)_2PbI_3$ vibrates along the *y*-direction, the I(7) atom of $Ag(NH_3)_2PbI_3$ vibrates along the *y*-direction, and the I(10) atom of $Au(NH_3)_2PbI_3$ vibrates along the *z*-direction. The three zero frequency translation modes at the Γ point could also be observed. Therefore, the proposed 3D lead iodide perovskites with complex ions are basically thermodynamically stable.

Then, the formation and dissociation energies of these lead iodide perovskites were calculated based on eqn (1) and (2),

$$E_{\text{formation}} = E_{\text{perovskite}} - E_{\text{Cu/Ag/Au}} - 2E_{\text{NH}_3} - E_{\text{Pb}} - \frac{3}{2}E_{\text{I}_2} \quad (1)$$

$$E_{\text{dissociation}} = E_{\text{PbI}_2} + E_{\text{CuI/AgI/AuI}} + 2E_{\text{NH}_3} - E_{\text{perovskite}} \quad (2)$$

where $E_{\text{perovskite}}$, E_{PbI_2}, E_{Pb}, $E_{\text{Cu/Ag/Au}}$, and $E_{\text{CuI/AgI/AuI}}$ are the energies of the 3D lead iodide perovskite, PbI_2, Pb atom, Cu (or Ag, or Au) atom, and CuI (or AgI, or AuI), respectively (PbI_2 and CuI/AgI/AuI were simulated as solid). E_{I_2} and E_{NH_3} are the energies of the isolated I_2 and NH_3 molecules, respectively. As shown in Table S2 (ESI†), all the lead iodide perovskites exhibit negative formation energies and positive dissociation energies,

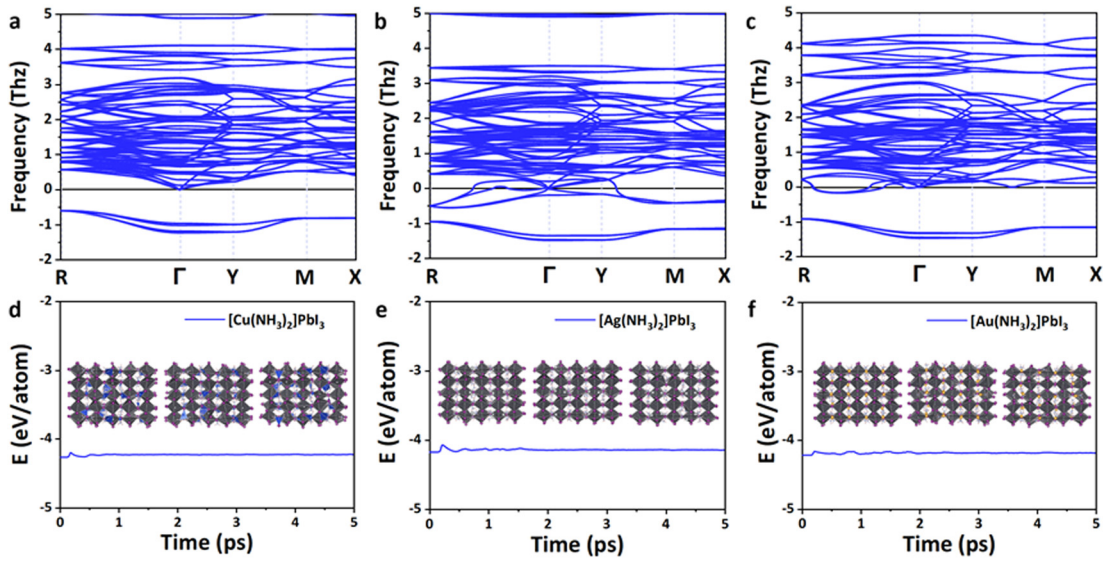

Fig. 3 The thermodynamic and kinetic stability of the proposed lead iodide perovskites. The phonon spectra of $Cu(NH_3)_2PbI_3$ (a), $Ag(NH_3)_2PbI_3$ (b) and $Au(NH_3)_2PbI_3$ (c) at 0 K. The energy fluctuation of $Cu(NH_3)_2PbI_3$ (d), $Ag(NH_3)_2PbI_3$ (e) and $Au(NH_3)_2PbI_3$ (f) supercells in the *ab initio* molecular dynamics simulations. The insets of (d)–(f) are the structures of $Cu(NH_3)_2PbI_3$ (d), $Ag(NH_3)_2PbI_3$ (e) and $Au(NH_3)_2PbI_3$ (f) during *ab initio* molecular dynamics simulations (AIMD) at 2.0, 3.5 and 5.0 ps.

which are similar in magnitude to those of α-phase $MAPbI_3$,[24] confirming the thermodynamic stability of the proposed lead iodide perovskites.

In order to further confirm the kinetic stability of these lead iodide perovskites, *ab initio* molecular dynamics simulations were then performed at 300 K for 5 ps. As shown in Fig. 3d–f, the energies of these 3D lead iodide perovskites fluctuate significantly in the first 2 ps but remain stable in the next 3 ps. The octahedral frameworks are not destroyed during the AIMD simulations for $Ag(NH_3)_2PbI_3$ and $Au(NH_3)_2PbI_3$, which indicates that these two perovskites are dynamically stable. However, the structure of $Cu(NH_3)_2PbI_3$ during AIMD simulation is destroyed, and Cu–I bonds are formed (Fig. S3, ESI†), which indicates that $Cu(NH_3)_2PbI_3$ is not kinetically stable. Based on the above discussions, $Ag(NH_3)_2PbI_3$ and $Au(NH_3)_2PbI_3$ are both thermodynamically and kinetically stable. Nevertheless, their suitability as a material platform for solar cells still needs further investigation.

Excellent solar cell materials should have an appropriate band gap, a high carrier mobility and a large optical absorption coefficient. Therefore, the electronic and optical properties of these lead iodide perovskites were further investigated. According to the Shockley–Queisser limit, the band gap of the best absorber should be in the optimal range of 0.85–1.85 eV; thus, the theoretical power conversion efficiency of solar cells could exceed 25%.[45] The band structures of these 3D perovskites are calculated based on the Perdew–Burke–Ernzerhof (PBE) functional[73] together with spin polarization and shown in Fig. 4 and Fig. S4–S7 (ESI†). The conduction band minimum (CBM) and valence band maximum (VBM) of $Ag(NH_3)_2PbI_3$ and $Au(NH_3)_2PbI_3$ are all located at the *Γ* point, which indicates that they exhibit direct band gaps. In contrast, $Cu(NH_3)_2PbI_3$ exhibits an indirect band gap with the CBM located at the *Γ* point and the VBM located at the *X* point. These three perovskites exhibit almost the same conduction bands with three degenerate conduction band minima near the *Γ* point (CB1, CB2 and CB3) but different valence bands. The valence band of $Cu(NH_3)_2PbI_3$ is almost flat, which could not facilitate hole transport. Among these perovskites, $Cu(NH_3)_2PbI_3$ exhibits the smallest band gap of 1.34 eV, while $Ag(NH_3)_2PbI_3$ and $Au(NH_3)_2PbI_3$ exhibit slightly larger band gaps of 1.65 eV and 1.70 eV, respectively. Since the energy of the Cu 3d orbit is distinctly lower than that of the Ag 4d and Au 5d orbits (Fig. S8, ESI†), it contributes mainly to the VBM of $Cu(NH_3)_2PbI_3$. Thus, $Cu(NH_3)_2PbI_3$ exhibits a different valence band compared with $Ag(NH_3)_2PbI_3$ and $Au(NH_3)_2PbI_3$. In order to ensure the reliability of our calculation, the electronic structures of these perovskites were also calculated by the Plane-Wave self-consistent field (PWscf) with the PBE functional considering the spin–orbit coupling (SOC) and the scalar relativistic (SR) effect,[74,75] and almost the same band gaps were obtained (1.33 eV, 1.62 eV and 1.64 eV for $Cu(NH_3)_2PbI_3$, $Ag(NH_3)_2PbI_3$ and $Au(NH_3)_2PbI_3$, respectively, Fig. S5, ESI†). However, while calculating the band structures with the PBE functional and considering the SOC only, the proposed perovskite exhibits a much smaller band gap (0.54 eV, 0.73 eV and 0.70 eV for $Cu(NH_3)_2PbI_3$, $Ag(NH_3)_2PbI_3$ and $Au(NH_3)_2PbI_3$, respectively, Fig. S6, ESI†) which may be due to the error compensation between the SOC and SR is transformed into the bandgap. On the other hand, the absorption coefficient is another important parameter for solar cells, and a direct band gap in the optimal absorption range does not always guarantee that it has a larger absorption coefficient. The absorption spectra of these three perovskites were then calculated and are shown in Fig. S9 (ESI†). $Cu(NH_3)_2PbI_3$, $Ag(NH_3)_2PbI_3$ and $Au(NH_3)_2PbI_3$ all have much larger absorption coefficients than that of α- and β-$MAPbI_3$ in the visible range, which indicates that these proposed 3D perovskites exhibit much stronger photon harvesting ability towards solar cell applications.[76] Moreover, the optical transition of these three perovskites was also estimated through calculating the transition dipole moment (TDM).[77,78] As shown in Fig. S10 (ESI†), the direct VB-CB transitions of

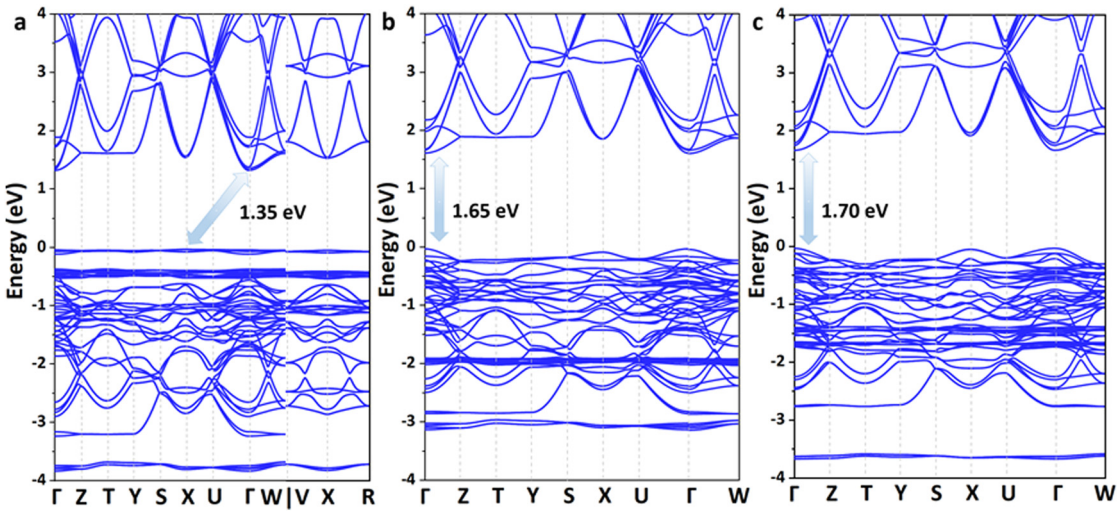

Fig. 4 The calculated band structures of the 3D perovskite with complex ions based on the PBE functional: $Cu(NH_3)_2PbI_3$ (a), $Ag(NH_3)_2PbI_3$ (b) and $Au(NH_3)_2PbI_3$ (c).

$Ag(NH_3)_2PbI_3$ and $Au(NH_3)_2PbI_3$ are more favorable than that of $Cu(NH_3)_2PbI_3$. Given the discussion of stability, band structures, absorption coefficients and optical transition, $Ag(NH_3)_2PbI_3$ and $Au(NH_3)_2PbI_3$ are good candidates towards high-performance perovskite solar cells.

The projected density of states (PDOS) of these 3D perovskites are further calculated and shown in Fig. S11 (ESI†). The VBM of $Cu(NH_3)_2PbI_3$ is mainly contributed by the Cu 3d orbit, while the CBM consists of the Pb 6p orbit and I 5p orbit. In contrast, the VBM of $Ag(NH_3)_2PbI_3$ is mainly contributed by both the I 5p orbit and Ag 4d orbit, while it is mainly contributed by the I 5p orbit for $Au(NH_3)_2PbI_3$. The CBM compositions of $Ag(NH_3)_2PbI_3$ and $Au(NH_3)_2PbI_3$ are similar to that of $Cu(NH_3)_2PbI_3$. Thus, the electronic transition of $Ag(NH_3)_2PbI_3$ should displace the electronic density from the A-site cation and I to Pb. For the electronic transition from the A-site cation to Pb, it is widely observed in low-dimensional perovskite with large conjugated cations.[27] This depends on the energy discrepancy between the VB (or HOMO) of the cation and the inorganic framework (as shown in Fig. S13, ESI†).[79] In order to further confirm the PDOS distribution of these perovskites, the electron densities at the VBM and CBM are calculated and shown in Fig. 5 and Fig. S15–S19 (ESI†). Consistent with the PDOS discussed above, the electron density at the VBM of $Cu(NH_3)_2PbI_3$ is mainly localized on the Cu atom, which is mainly located on the I atom and Ag atom for $Ag(NH_3)_2PbI_3$, and only on the I atom for $Au(NH_3)_2PbI_3$, respectively. Meanwhile, the electron densities of $Ag(NH_3)_2PbI_3$ and $Au(NH_3)_2PbI_3$ at CBM1, CBM2 and CBM3 consist of the Pb 6p orbit and I 5p orbit (Fig. S15–S17, ESI†). As shown in Fig. 5d–f, the electron densities (the planes sliced for the electron densities are shown in Fig. S14, ESI†) at the CBM of $Ag(NH_3)_2PbI_3$ and $Au(NH_3)_2PbI_3$ demonstrate that the electron clouds indeed disperse along the Pb–I skeleton in three directions, which indicates an isotropic electron transport feature and 3D electronic connectivity. Different from the transport of electrons, holes are moving along the halide → complex ion → halide direction. Therefore, $Ag(NH_3)_2PbI_3$ and $Au(NH_3)_2PbI_3$ are not only structural 3D but also electronic 3D, which is further confirmed by the effective electron and hole masses discussed below. The spin polarization was also considered while calculating the band structure and DOS, and the same results were obtained for spin-up and spin-down (as shown in Fig. S7 and S10, ESI†).

The electron and hole effective masses of these 3D lead iodide perovskites are then calculated based on eqn (3),

$$\frac{1}{m^*} = \frac{1}{\hbar^2}\frac{\partial^2 E}{\partial k^2} \tag{3}$$

where m^* is the effective mass and $\hbar$ is the reduced Planck constant. Since these perovskites have three almost degenerated CBMs near the Γ point, three electron effective masses (m_e^*) and their harmonic mean values are calculated from Γ to T, Γ to W and Γ to X corresponding to the three directions of

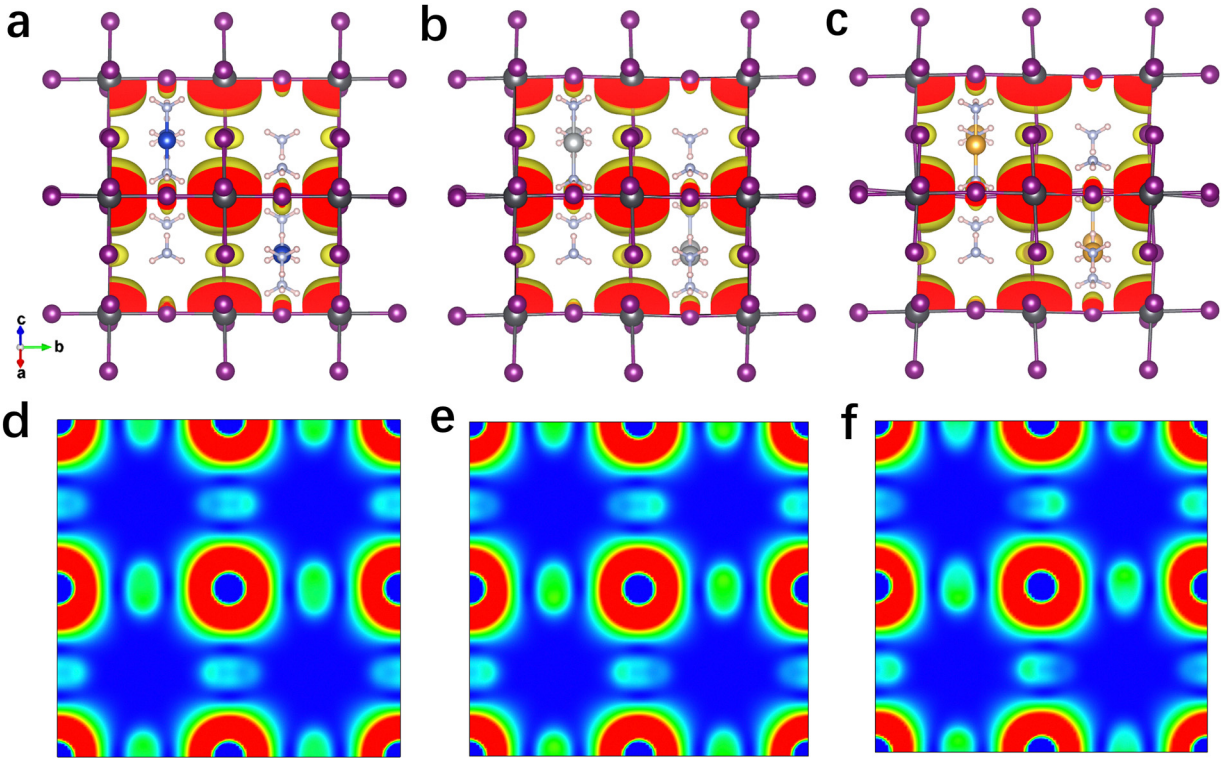

Fig. 5 Sum of the electron density of the degenerated CBMs of the proposed 3D perovskites with complex ions. Isosurface plot of the 3D CBM electron density (isovalue = 0.0008 e $Bohr^{-3}$) of $Cu(NH_3)_2PbI_3$ (a), $Ag(NH_3)_2PbI_3$ (b), and $Au(NH_3)_2PbI_3$ (c). 2D CBM charge density maps on the (101) plane of $Cu(NH_3)_2PbI_3$ (d), $Ag(NH_3)_2PbI_3$ (e) and $Au(NH_3)_2PbI_3$ (f).

the inorganic perovskite framework (Table S5 and Fig. S21–S24, ESI†). Among these three directions, the minimal electron effective masses among the degenerated CBs (0.25 m_e, 0.26 m_e and 0.27 m_e) as well as their harmonic mean electron effective masses are of the same magnitude (0.66 m_e, 0.72 m_e and 0.69 m_e) for $Cu(NH_3)_2PbI_3$, $Ag(NH_3)_2PbI_3$ and $Au(NH_3)_2PbI_3$, respectively, which further confirms the isotropic electron transport feature and 3D electronic connectivity of these three perovskites. The hole effective masses and their harmonic mean values of these perovskites along the inorganic perovskite framework (from Γ to T, Γ to W and Γ to X for $Ag(NH_3)_2PbI_3$ and $Au(NH_3)_2PbI_3$, respectively, and from X to V, X to R and X to Γ for $Cu(NH_3)_2PbI_3$) were also calculated. The hole effective masses along the Γ–X direction of $Ag(NH_3)_2PbI_3$ (31.63 m_e) and $Au(NH_3)_2PbI_3$ (23.64 m_e) are much larger than other directions ($\sim$2.90 m_e for $Ag(NH_3)_2PbI_3$ and 2.55 m_e for $Ag(NH_3)_2PbI_3$), which is similar to that of γ-$MAPbI_3$ (11.98 m_e for [010] *vs.* 1.18 m_e for [100] and 1.05 m_e for [001] direction).[76,80] In contrast, $Cu(NH_3)_2PbI_3$ shows large harmonic mean hole effective masses along all three directions, Γ–T (19.59 m_e), Γ–W (19.62 m_e) and Γ–X (9.7 m_e).[76] Therefore, based on the hole effective masses (Table S5 and Fig. S21, ESI†) and charge density mapping as discussed above, it is confirmed that $Ag(NH_3)_2PbI_3$ and $Au(NH_3)_2PbI_3$ exhibit a 2D hole transport feature, while $Cu(NH_3)_2PbI_3$ could not facilitate hole transport in all three directions. This is also consistent with the flat valence band of $Cu(NH_3)_2PbI_3$, as shown in Fig. 4a. The 2D hole transport feature of $Ag(NH_3)_2PbI_3$ and $Au(NH_3)_2PbI_3$ may originate from the linear profile of the cations. The cations are arranging in the *xz* plane (Fig. 2) and holes are moving along the halide → complex ion → halide direction. Thus, $Ag(NH_3)_2PbI_3$ and $Au(NH_3)_2PbI_3$ exhibit anisotropic hole transport (Fig. S23, ESI†). Based on the above discussion, $Cu(NH_3)_2PbI_3$ could not be adopted as the light absorber of solar cells owing to both poorer stability and slower hole transport. Meanwhile, $Ag(NH_3)_2PbI_3$ and $Au(NH_3)_2PbI_3$ exhibit a modest harmonic mean hole and electron effective mass together with optimized band gaps and large absorption coefficients, which is promising towards application in high-performance perovskite solar cells.[76]

Conclusions

In summary, 3D lead iodide perovskites based on complex ions, $Cu(NH_3)_2PbI_3$, $Ag(NH_3)_2PbI_3$ and $Au(NH_3)_2PbI_3$, are demonstrated for the first time in this work. $Ag(NH_3)_2PbI_3$ and $Au(NH_3)_2PbI_3$ are found to be both kinetically and thermodynamically stable based on structural optimization, phonon spectra, *ab initio* molecular dynamics simulations, formation and dissociation energies. In particular, $Ag(NH_3)_2PbI_3$ and $Au(NH_3)_2PbI_3$ are not only structural 3D but also electronic 3D. Moreover, these two perovskites exhibit large absorption coefficients, suitable band gaps, and small hole and electron masses, which are very promising towards application in perovskite solar cells. These findings could throw light on the development of novel electronic 3D perovskites with superior optical and electrical properties.

Conflicts of interest

There are no conflicts to declare.

Acknowledgements

G. Long, H. Wang, H. Lu and T. Wang acknowledge the financial support from the NSFC (52103218, 92256202, 12261131500) of China, the Fundamental Research Funds for the Central Universities, Nankai University (Grant Number: 023-63233038), and the Opening Project of State Key Laboratory of Polymer Materials Engineering (Sichuan University) (Grant No. sklpme2021-05-02). Y. Zhou and Y. Yu thank the funding from NSFC (No. 22103097) of China, The Science and Technology Bureau of Guangzhou (grant No. 202102020495). X. Wei acknowledges the financial support from the National Key R&D Program of China (2017YFE0131900). All theoretical calculations were performed at the National Supercomputer Center in Guangzhou.

Notes and references

1 M. Grätzel, *Nat. Mater.*, 2014, **13**, 838–842.
2 J. Jeong, M. Kim, J. Seo, H. Lu, P. Ahlawat, A. Mishra, Y. Yang, M. A. Hope, F. T. Eickemeyer, M. Kim, Y. J. Yoon, I. W. Choi, B. P. Darwich, S. J. Choi, Y. Jo, J. H. Lee, B. Walker, S. M. Zakeeruddin, L. Emsley, U. Rothlisberger, A. Hagfeldt, D. S. Kim, M. Grätzel and J. Y. Kim, *Nature*, 2021, **592**, 381–385.
3 N. J. Jeon, H. Na, E. H. Jung, T.-Y. Yang, Y. G. Lee, G. Kim, H.-W. Shin, S. Il Seok, J. Lee and J. Seo, *Nat. Energy*, 2018, **3**, 682–689.
4 H. Tsai, W. Nie, J.-C. Blancon, C. C. Stoumpos, R. Asadpour, B. Harutyunyan, A. J. Neukirch, R. Verduzco, J. J. Crochet, S. Tretiak, L. Pedesseau, J. Even, M. A. Alam, G. Gupta, J. Lou, P. M. Ajayan, M. J. Bedzyk, M. G. Kanatzidis and A. D. Mohite, *Nature*, 2016, **536**, 312–316.
5 D. Bi, C. Yi, J. Luo, J.-D. Décoppet, F. Zhang, S. M. Zakeeruddin, X. Li, A. Hagfeldt and M. Grätzel, *Nat. Energy*, 2016, **1**, 16142.
6 E. Eperon Giles, T. Leijtens, A. Bush Kevin, R. Prasanna, T. Green, T.-W. Wang Jacob, P. McMeekin David, G. Volonakis, L. Milot Rebecca, R. May, A. Palmstrom, J. Slotcavage Daniel, A. Belisle Rebecca, B. Patel Jay, S. Parrott Elizabeth, J. Sutton Rebecca, W. Ma, F. Moghadam, B. Conings, A. Babayigit, H.-G. Boyen, S. Bent, F. Giustino, M. Herz Laura, B. Johnston Michael, D. McGehee Michael and J. Snaith Henry, *Science*, 2016, **354**, 861–865.
7 J. Bie, D.-B. Yang, M.-G. Ju, Q. Pan, Y.-M. You, W. Fa, X. C. Zeng and S. Chen, *JACS Au*, 2021, **1**, 475–483.
8 J. Dai, L. Ma, M. Ju, J. Huang and X. C. Zeng, *Phys. Chem. Chem. Phys.*, 2017, **19**, 21691–21695.
9 W. Xu, Q. Hu, S. Bai, C. Bao, Y. Miao, Z. Yuan, T. Borzda, A. J. Barker, E. Tyukalova, Z. Hu, M. Kawecki, H. Wang,

Z. Yan, X. Liu, X. Shi, K. Uvdal, M. Fahlman, W. Zhang, M. Duchamp, J.-M. Liu, A. Petrozza, J. Wang, L.-M. Liu, W. Huang and F. Gao, *Nat. Photonics*, 2019, **13**, 418–424.
10 S. Yun, X. Zhou, J. Even and A. Hagfeldt, *Angew. Chem., Int. Ed.*, 2017, **56**, 15806–15817.
11 W. Yan, Z. Wang, Y. Gong, S. Guo, J. Jiang, J. Chen, C. Tang, R. Xia, W. Huang and H. Xin, *Org. Electron.*, 2019, **67**, 208–214.
12 Z. Xiao, Z. Song and Y. Yan, *Adv. Mater.*, 2019, **31**, 1803792.
13 M. Yuan, L. N. Quan, R. Comin, G. Walters, R. Sabatini, O. Voznyy, S. Hoogland, Y. Zhao, E. M. Beauregard, P. Kanjanaboos, Z. Lu, D. H. Kim and E. H. Sargent, *Nat. Nanotechnol.*, 2016, **11**, 872–877.
14 R. Fu, W. Zhao, L. Wang, Z. Ma, G. Xiao and B. Zou, *Angew. Chem., Int. Ed.*, 2021, **60**, 10082–10088.
15 V. Adinolfi, O. Ouellette, M. I. Saidaminov, G. Walters, A. L. Abdelhady, O. M. Bakr and E. H. Sargent, *Adv. Mater.*, 2016, **28**, 7264–7268.
16 H. Wei and J. Huang, *Nat. Commun.*, 2019, **10**, 1066.
17 Q. Lin, A. Armin, P. L. Burn and P. Meredith, *Nat. Photonics*, 2015, **9**, 687–694.
18 S. Yakunin, D. N. Dirin, Y. Shynkarenko, V. Morad, I. Cherniukh, O. Nazarenko, D. Kreil, T. Nauser and M. V. Kovalenko, *Nat. Photonics*, 2016, **10**, 585–589.
19 W. Yu, F. Li, L. Yu, M. R. Niazi, Y. Zou, D. Corzo, A. Basu, C. Ma, S. Dey, M. L. Tietze, U. Buttner, X. Wang, Z. Wang, M. N. Hedhili, C. Guo, T. Wu and A. Amassian, *Nat. Commun.*, 2018, **9**, 5354.
20 H. Zhu, Y. Fu, F. Meng, X. Wu, Z. Gong, Q. Ding, M. V. Gustafsson, M. T. Trinh, S. Jin and X. Y. Zhu, *Nat. Mater.*, 2015, **14**, 636–642.
21 Y. Jia, R. A. Kerner, A. J. Grede, B. P. Rand and N. C. Giebink, *Nat. Photonics*, 2017, **11**, 784–788.
22 J. Y. Kim, J.-W. Lee, H. S. Jung, H. Shin and N.-G. Park, *Chem. Rev.*, 2020, **120**, 7867–7918.
23 W.-J. Yin, T. Shi and Y. Yan, *J. Phys. Chem. C*, 2015, **119**, 5253–5264.
24 G. Long, Y. Zhou, M. Zhang, R. Sabatini, A. Rasmita, L. Huang, G. Lakhwani and W. Gao, *Adv. Mater.*, 2019, **31**, 1807628.
25 Z.-J. Wang, L.-K. Wu, N. Wang, Q.-Q. Hu, J.-R. Li and H.-Y. Ye, *Dalton Trans.*, 2023, **52**, 2799–2803.
26 G. Long, C. Jiang, R. Sabatini, Z. Yang, M. Wei, L. N. Quan, Q. Liang, A. Rasmita, M. Askerka, G. Walters, X. Gong, J. Xing, X. Wen, R. Quintero-Bermudez, H. Yuan, G. Xing, X. R. Wang, D. Song, O. Voznyy, M. Zhang, S. Hoogland, W. Gao, Q. Xiong and E. H. Sargent, *Nat. Photonics*, 2018, **12**, 528–533.
27 Y. Gao, E. Shi, S. Deng, S. B. Shiring, J. M. Snaider, C. Liang, B. Yuan, R. Song, S. M. Janke, A. Liebman-Peláez, P. Yoo, M. Zeller, B. W. Boudouris, P. Liao, C. Zhu, V. Blum, Y. Yu, B. M. Savoie, L. Huang and L. Dou, *Nat. Chem.*, 2019, **11**, 1151–1157.
28 T. M. Koh, B. Febriansyah and N. Mathews, *Chemistry*, 2017, **2**, 326–327.
29 D. Fu, Z. Hou, Y. He, J.-C. Liu, H.-P. Lv and Y.-Y. Tang, *Chem. Mater.*, 2022, **34**, 3518–3524.
30 H. Wang, J. Li, H. Lu, S. Gull, T. Shao, Y. Zhang, T. He, Y. Chen, T. He and G. Long, *Angew. Chem., Int. Ed.*, 2023, e202309600.
31 R. Zhang, X. Mao, Y. Yang, S. Yang, W. Zhao, T. Wumaier, D. Wei, W. Deng and K. Han, *Angew. Chem., Int. Ed.*, 2019, **58**, 2725–2729.
32 X.-G. Zhao, J.-H. Yang, Y. Fu, D. Yang, Q. Xu, L. Yu, S.-H. Wei and L. Zhang, *J. Am. Chem. Soc.*, 2017, **139**, 2630–2638.
33 G. Long, R. Sabatini, M. I. Saidaminov, G. Lakhwani, A. Rasmita, X. Liu, E. H. Sargent and W. Gao, *Nat. Rev. Mater.*, 2020, **5**, 423–439.
34 L. Etgar, *Energy Environ. Sci.*, 2018, **11**, 234–242.
35 K. Drużbicki, R. Lavén, J. Armstrong, L. Malavasi, F. Fernandez-Alonso and M. Karlsson, *J. Phys. Chem. Lett.*, 2021, **12**, 3503–3508.
36 A. Amat, E. Mosconi, E. Ronca, C. Quarti, P. Umari, M. K. Nazeeruddin, M. Grätzel and F. De Angelis, *Nano Lett.*, 2014, **14**, 3608–3616.
37 C. Motta, F. El-Mellouhi, S. Kais, N. Tabet, F. Alharbi and S. Sanvito, *Nat. Commun.*, 2015, **6**, 7026.
38 K. Drużbicki, R. S. Pinna, S. Rudić, M. Jura, G. Gorini and F. Fernandez-Alonso, *J. Phys. Chem. Lett.*, 2016, **7**, 4701–4709.
39 A. Filippetti, P. Delugas, M. I. Saba and A. Mattoni, *J. Phys. Chem. Lett.*, 2015, **6**, 4909–4915.
40 A. Ray, B. Martín-García, A. Moliterni, N. Casati, K. M. Boopathi, D. Spirito, L. Goldoni, M. Prato, C. Giacobbe, C. Giannini, F. Di Stasio, R. Krahne, L. Manna and A. L. Abdelhady, *Adv. Mater.*, 2022, **34**, 2106160.
41 G. Saleh, G. Biffi, F. Di Stasio, B. Martín-García, A. L. Abdelhady, L. Manna, R. Krahne and S. Artyukhin, *Chem. Mater.*, 2021, **33**, 8524–8533.
42 K. Frohna, T. Deshpande, J. Harter, W. Peng, B. A. Barker, J. B. Neaton, S. G. Louie, O. M. Bakr, D. Hsieh and M. Bernardi, *Nat. Commun.*, 2018, **9**, 1829.
43 Z. Xiao, W. Meng, J. Wang, D. B. Mitzi and Y. Yan, *Mater. Horiz.*, 2017, **4**, 206–216.
44 G. E. Eperon, S. D. Stranks, C. Menelaou, M. B. Johnston, L. M. Herz and H. J. Snaith, *Energy Environ. Sci.*, 2014, **7**, 982–988.
45 W. Shockley and H. J. Queisser, *J. Appl. Phys.*, 1961, **32**, 510–519.
46 M. R. Filip, S. Hillman, A. A. Haghighirad, H. J. Snaith and F. Giustino, *J. Phys. Chem. Lett.*, 2016, **7**, 2579–2585.
47 A. H. Slavney, T. Hu, A. M. Lindenberg and H. I. Karunadasa, *J. Am. Chem. Soc.*, 2016, **138**, 2138–2141.
48 E. T. McClure, M. R. Ball, W. Windl and P. M. Woodward, *Chem. Mater.*, 2016, **28**, 1348–1354.
49 F. Wei, Z. Deng, S. Sun, F. Xie, G. Kieslich, D. M. Evans, M. A. Carpenter, P. D. Bristowe and A. K. Cheetham, *Mater. Horiz.*, 2016, **3**, 328–332.
50 M. T. Sirtl, R. Hooijer, M. Armer, F. G. Ebadi, M. Mohammadi, C. Maheu, A. Weis, B. T. van Gorkom, S. Häringer, R. A. J. Janssen, T. Mayer, V. Dyakonov, W. Tress and T. Bein, *Adv. Energy Mater.*, 2022, **12**, 2103215.
51 H.-Y. Zhang, X.-G. Chen, Z.-X. Zhang, X.-J. Song, T. Zhang, Q. Pan, Y. Zhang and R.-G. Xiong, *Adv. Mater.*, 2020, **32**, 2005213.

52 Ma Mączka, M. Ptak, A. Gągor, D. Stefańska, J. K. Zaręba and A. Sieradzki, *Chem. Mater.*, 2020, **32**, 1667–1673.
53 S. Huang, P. Huang, L. Wang, J. Han, Y. Chen and H. Zhong, *Adv. Mater.*, 2019, **31**, 1903830.
54 H.-Y. Zhang, X.-J. Song, H. Cheng, Y.-L. Zeng, Y. Zhang, P.-F. Li, W.-Q. Liao and R.-G. Xiong, *J. Am. Chem. Soc.*, 2020, **142**, 4604–4608.
55 X. Li, Y. He, M. Kepenekian, P. Guo, W. Ke, J. Even, C. Katan, C. C. Stoumpos, R. D. Schaller and M. G. Kanatzidis, *J. Am. Chem. Soc.*, 2020, **142**, 6625–6637.
56 Y.-Y. Tang, Y.-H. Liu, H. Peng, B.-B. Deng, T.-T. Cheng and Y.-T. Hu, *J. Am. Chem. Soc.*, 2020, **142**, 19698–19704.
57 D. Umeyama, L. Leppert, B. A. Connor, M. A. Manumpil, J. B. Neaton and H. I. Karunadasa, *Angew. Chem., Int. Ed.*, 2020, **59**, 19087–19094.
58 P. Fu, S. Hu, J. Tang and Z. Xiao, *Front. Optoelectron.*, 2021, **14**, 252–259.
59 X. Li, M. Kepenekian, L. Li, H. Dong, C. C. Stoumpos, R. Seshadri, C. Katan, P. Guo, J. Even and M. G. Kanatzidis, *J. Am. Chem. Soc.*, 2022, **144**, 3902–3912.
60 C. J. Bartel, C. Sutton, B. R. Goldsmith, R. Ouyang, C. B. Musgrave, L. M. Ghiringhelli and M. Scheffler, *Sci. Adv.*, 2019, **5**, eaav0693.
61 A. E. Fedorovskiy, N. A. Drigo and M. K. Nazeeruddin, *Small Methods*, 2020, **4**, 1900426.
62 N. A. Benedek and C. J. Fennie, *J. Phys. Chem. C*, 2013, **117**, 13339–13349.
63 I. P. Swainson, C. Stock, S. F. Parker, L. Van Eijck, M. Russina and J. W. Taylor, *Phys. Rev. B: Condens. Matter Mater. Phys.*, 2015, **92**, 100303.
64 F. Brivio, J. M. Frost, J. M. Skelton, A. J. Jackson, O. J. Weber, M. T. Weller, A. R. Goñi, A. M. A. Leguy, P. R. F. Barnes and A. Walsh, *Phys. Rev. B: Condens. Matter Mater. Phys.*, 2015, **92**, 144308.
65 A. Marronnier, G. Roma, S. Boyer-Richard, L. Pedesseau, J.-M. Jancu, Y. Bonnassieux, C. Katan, C. C. Stoumpos, M. G. Kanatzidis and J. Even, *ACS Nano*, 2018, **12**, 3477–3486.
66 A. N. Beecher, O. E. Semonin, J. M. Skelton, J. M. Frost, M. W. Terban, H. Zhai, A. Alatas, J. S. Owen, A. Walsh and S. J. L. Billinge, *ACS Energy Lett.*, 2016, **1**, 880–887.
67 I. Maeng, S. Lee, H. Tanaka, J.-H. Yun, S. Wang, M. Nakamura, Y.-K. Kwon and M.-C. Jung, *NPG Asia Mater.*, 2020, **12**, 53.
68 A. M. A. Leguy, A. R. Goñi, J. M. Frost, J. Skelton, F. Brivio, X. Rodríguez-Martínez, O. J. Weber, A. Pallipurath, M. I. Alonso, M. Campoy-Quiles, M. T. Weller, J. Nelson, A. Walsh and P. R. F. Barnes, *Phys. Chem. Chem. Phys.*, 2016, **18**, 27051–27066.
69 C. Gehrmann and D. A. Egger, *Nat. Commun.*, 2019, **10**, 3141.
70 T. Sun, D.-B. Zhang and R. M. Wentzcovitch, *Phys. Rev. B: Condens. Matter Mater. Phys.*, 2014, **89**, 094109.
71 O. Hellman, I. A. Abrikosov and S. I. Simak, *Phys. Rev. B: Condens. Matter Mater. Phys.*, 2011, **84**, 180301.
72 R. Comin, M. K. Crawford, A. H. Said, N. Herron, W. E. Guise, X. Wang, P. S. Whitfield, A. Jain, X. Gong, A. J. H. McGaughey and E. H. Sargent, *Phys. Rev. B*, 2016, **94**, 094301.
73 J. P. Perdew, A. Ruzsinszky, G. I. Csonka, O. A. Vydrov, G. E. Scuseria, L. A. Constantin, X. Zhou and K. Burke, *Phys. Rev. Lett.*, 2008, **100**, 136406.
74 E. Mosconi, P. Umari and F. De Angelis, *Phys. Chem. Chem. Phys.*, 2016, **18**, 27158–27164.
75 P. Umari, E. Mosconi and F. De Angelis, *Sci. Rep.*, 2014, **4**, 4467.
76 Y. Zhou, F. Huang, Y.-B. Cheng and A. Gray-Weale, *Phys. Chem. Chem. Phys.*, 2015, **17**, 22604–22615.
77 Z. Wang, A. M. Ganose, C. Niu and D. O. Scanlon, *J. Mater. Chem. C*, 2019, **7**, 5139–5147.
78 W. Meng, X. Wang, Z. Xiao, J. Wang, D. B. Mitzi and Y. Yan, *J. Phys. Chem. Lett.*, 2017, **8**, 2999–3007.
79 Y. Gao, Z. Wei, S.-N. Hsu, B. W. Boudouris and L. Dou, *Mater. Chem. Front.*, 2020, **4**, 3400–3418.
80 J. Feng and B. Xiao, *J. Phys. Chem. Lett.*, 2014, **5**, 1278–1282.